ELSEVIER

Physica D 166 (2002) 155–166

PHYSICA D

www.elsevier.com/locate/physd

Influence of lateral boundary conditions on a phase-defect description of traveling-wave convection patterns

C.M. Aegerter[1], C.M. Surko*

Department of Physics, University of California San Diego, 9500 Gilman Drive, La Jolla, CA 92093-0319, USA

Received 26 January 2001; received in revised form 1 March 2002; accepted 4 March 2002
Communicated by R.P. Behringer

Abstract

Traveling-wave convection patterns in binary fluid mixtures of ethanol and water have been studied experimentally in containers with lateral boundaries of different shapes, including circular cells of two different sizes, rectangular and stadium-shaped cells. The nature of the patterns depends qualitatively upon the shape of the lateral boundaries. This paper analyzes these patterns in terms of topological phase defects in the complex order parameter, providing a reduced description of the system. The experimentally measured phase fields (and hence the patterns) can be reconstructed from the location and charge of the topological defects. For good agreement with experiment, the structure of individual defects is found to depend on both nearest-neighbor interactions of like-sign defects and the global structure of the patterns, reflected by the net charge of the defects. Further implications of these results for understanding traveling-wave patterns and dynamics are discussed.

PACS: 47.54.+r; 47.27.Te; 47.52.+j

Keywords: Traveling wave; Phase defect; Convection patterns

1. Introduction

Non-equilibrium systems are commonplace in our physical world. It is fair to say that understanding and controlling the behavior of such systems driven far from thermodynamic equilibrium is important in many, if not most areas of science and engineering [1,2]. Phenomena that have received attention in recent years range from technologically important problems in areas of engineering and biology to fundamental studies of model physical systems. Topics in the latter category include studies of granular materials [3], convection in fluids [4,5], wave and pulse phenomena in chemical reactors [6,7], and driven magnetic vortices in superconductors [8,9]. Problems of practical interest include studies of optical patterns in large aspect ratio lasers [10], population dynamics in epidemiology and ecology [11,12], pattern formation in bacterial colonies [13,14], and studies of the dynamics of the heart [15]. A fascinating observation that drives much scientific interest is that phenomena exhibited in many of these systems are remarkably similar in spite of the fact that the underlying physical systems are very different [1]. Thus, a unifying description of many of these phenomena may be possible, likely

* Corresponding author. Tel.: +1-858-534-6880; fax: +1-858-534-0173.
E-mail address: csurko@ucsd.edu (C.M. Surko).
[1] Present address: Department of Physics and Astronomy, Vrije Universiteit, 1081HV Amsterdam, The Netherlands.

0167-2789/02/$ – see front matter
PII: S0167-2789(02)00448-7

exploiting concepts developed in nonlinear dynamics. Due to the disparate microscopic origins of the patterns, a phenomenological approach has proven useful, describing the patterns and dynamics in terms of an order parameter. Such a description can describe a limited set of modes, excited in the system when it is driven from equilibrium [1,16]. Alternatively, in cases in which patterns display a high degree of regularity, the patterns can sometimes be described in terms of defects in an otherwise regular pattern [17,18]. In the case of the complex Ginzburg–Landau equation, progress has been made in developing a reduced description in terms of defects in the phase field [19] (also called vortices [20]). In this 'particle-field' description, the dynamics of the defects are given by the local values of the phase field, obtained from the defect positions, as a linear superposition of the contributions of all of the defects [19].

Here we deal with convection in binary fluid mixtures, which provides a model system for studying non-equilibrium traveling-wave phenomena. In particular, one can exploit the high degree of control that is attainable in convection experiments [21], as well as the fact that, at least in principal, theoretical models can be firmly based on the Navier–Stokes equation [4]. In an important range of parameters, this system can exhibit quasi-linear traveling waves which have been successfully described by model equations [16,22].

Recently, there has been progress in developing a 'particle-field' description of patterns and dynamics in binary fluid convection [23,29]. In that work, patterns in a circular cell were reconstructed from the locations of the phase defects, and the dynamics were described in terms of the local wave vector at a defect imposed by the phase field of all the other defects. The work described here focuses again on the patterns in this system, but seeks a more general description, capable of treating patterns in convection cells having a variety of shapes, including circular cells of different sizes, and rectangular and stadium-shaped cells.

The patterns in circular cells were found to rotate globally, meaning that the direction of the wavevector performs a complete, 2π rotation along the boundary of the cell. This breaking of chiral symmetry of the patterns is apparently due to the fact that sources of waves on the boundary of the circular cell are unstable. In these globally rotating states, the phase defects were found to have a non-zero pitch. In this paper, a variety of patterns are considered, including those which rotate globally (i.e., in the circular and stadium cells) and those which do not (in the stadium and rectangular cells). It is found that reconstruction of these patterns can also be achieved at the level of those done earlier for patterns in the circular cell. In the more general case considered here, the pitch parameter of globally rotating patterns must be augmented by a second parameter to describe breaking of (x, y) symmetry (e.g., in non-rotating patterns). Furthermore, an approximate scaling relationship is found between these two parameters and the total charge of defects on the cell boundary.

The simple, empirical parameterization presented here describes the main features of all the patterns observed in all the convection cells studied. It is important to emphasize however that there is, at this point, no theoretical justification for this description. In particular, a rigorous foundation of a 'particle-field' description of binary fluid convection remains to be developed. Nevertheless, given the potential gain in predictive capabilities of such a reduced model, it appears to be worthwhile to pursue this approach. Hopefully the reconstruction procedures described below can provide insights toward a theory of patterns and dynamics in this and similar non-equilibrium traveling-wave systems.

The remainder of this paper is organized as follows: in Section 2 we present a brief overview of the aspects of convection in fluid mixtures relevant to the experiments considered here. For more detailed accounts, we refer the reader to Ref. [5] for a concise theoretical model and to Ref. [24] for a more complete description experimental procedures. Directly relevant aspects of the experiment, such as the identification and tracking topological defects in the phase field as well as a phenomenological treatment of the structure of the phase field that is used in the reconstructions are described in Section 3. Section 4 describes the results of reconstructions of the phase field and the arrangements of phase defects observed in the different convection cells studied. In this section, we focus particularly on

the connection between locally imposed wavevectors at individual phase defects and the global structure of the patterns. In Section 5, we conclude with a summary describing relationships between the adjustable parameters in the model used and the statistics of defects in the different cells. Finally, we present a brief look to the future of work in this area.

2. Binary fluid convection

When convection occurs in a mixture instead of a pure fluid, qualitatively new phenomena can arise. This is due to the addition of the concentration as a second diffusing quantity [5,25]. In cases where the Soret effect is important, the two diffusing fields (temperature and concentration) are coupled [26]. For the parameters of the fluid mixture studied here, this coupling changes the initial instability from a stationary pitch-fork bifurcation into a sub-critical Hopf bifurcation [2,25]. The system can be described in terms of four parameters: the Rayleigh number, the separation ratio, and the Prandtl and Lewis numbers. The Rayleigh number, R, is a measure for the thermal driving and is given by the ratio of the buoyancy force due to the temperature difference and the dissipative force due to viscosity [4]:

$$R = \frac{g\alpha h^3 \Delta T}{\nu\kappa}, \tag{1}$$

where α is the thermal expansion coefficient, ν the kinematic viscosity, κ the thermal diffusivity, h the height of the fluid layer, ΔT the imposed temperature difference, and g the acceleration due to gravity. A second parameter is the separation ratio, ψ, which is a measure of the driving of convection due to Soret-induced concentration difference to that due to thermal expansion [25]:

$$\psi = -C(1-C)S_t \frac{\beta}{\alpha}, \tag{2}$$

where $\beta = \rho^{-1}(\partial\rho/\partial C)$ is the solutal expansion coefficient, C the concentration, and S_t the Soret coefficient.

The fluid studied here was a mixture of 8% ethanol in water (by weight), which at a mean temperature of 25 °C, corresponds to $\psi = -0.24$ [27]. The critical Rayleigh numbers (scaled by the value for the pure fluid R_0) are measured to be onset at $r_{co} = R_{co}/R_0 = 1.4$ and the saddle node at $r_s = 1.23$.

3. The experiment and analysis techniques

3.1. Description of the experiment

The experimental apparatus and procedures used here are similar to those described in detail in Ref. [28]. Additional modifications to the experiment, which were also used in the present work, are described in Ref. [24]. The convecting fluid is enclosed in a cell of height $h = 4$ mm with a silicon bottom plate and a sapphire top plate chosen for their large thermal conductivities. Feedback loops control the temperature of the plates such that the temperature difference is homogeneous across the cell to within 2 mK and stable in time to better than 1 mK. Patterns were visualized with a white light shadowgraph and images were recorded using a CCD camera which was controlled by a PC via a GPIB bus. In the remainder of this paper, times and distances are given in the natural units of the vertical thermal diffusion time ($\tau = h^2/\kappa = 124$ s) and the cell height ($h = 4$ mm), respectively [27].

The visualized patterns are treated as the real part of a complex order parameter, which is determined by the procedures described in Ref. [24].

3.2. Determination of the phase defects

A previous investigation of traveling-wave patterns in binary fluid convection described the patterns in terms of topological defects of the phase field [23,24,29]. Here we briefly discuss the procedures used to identify these defects from the phase fields. The basic analysis of the patterns including the determination of the phase field from the measured images is discussed in Ref. [24], where the algorithms used are described in detail. The determination of the locations and charges of these defects is important in describing both the patterns and the dynamics of the patterns. Strictly speaking, a topological defect is

a singularity, at which the phase is undefined. This corresponds to a crossing of zeros in the real and imaginary parts of the order parameter. In practice, a reliable determination using such a definition is unsuitable due to the discrete nature of the images [24,29]. Therefore, we base our determination of defect location on the topological constraint that a contour integral around a closed loop is zero unless that loop contains a defect. Specifically:

$$\oint \vec{\nabla}\phi \cdot \mathrm{d}\vec{s} = 2\pi c, \tag{3}$$

where c is the topological charge of the enclosed defect. This charge indicates the sign of the phase change along the contour. Thus, following the contour counterclockwise, $c > 0$ ($c < 0$) corresponds to an increase (decrease) in the phase from $-\pi$ to π (π to $-\pi$). An example of a defect map determined in this way is shown in Fig. 1, together with the corresponding phase field.

3.3. Reconstruction of patterns

As mentioned in Section 1, the reconstruction of the phase field from information about the locations of defects is necessary for a 'particle-field' description of a non-equilibrium system. Such a description, if successful, would be a tremendous simplification, reducing the dynamics of the entire pattern to a many-body problem concerned with just the phase defects [19]. Progress has been made using this strategy to describe patterns in binary fluid convection [23]; however in that work, it was found that the individual defects had to be given an additional structure to obtain good reconstructions. Here we will consider this question further. To describe patterns in cells of different shapes, we find that it is necessary to link the structure of individual defects to the global structure of the patterns. The focus of this paper is finding an appropriate structure of defects capable of describing patterns in cells with qualitatively different shapes.

To begin with, we will be concerned with understanding the local structure of a single phase defect. To a first approximation, in Cartesian coordinates, the phase at point (x, y) of a defect at $(x_\mathrm{d}, y_\mathrm{d})$ is given by the angle as measured from the defect's position multiplied by the topological charge of the defect

$$\phi_\mathrm{d}(x, y) = c\theta_\mathrm{d}(x, y) = c \cdot \tan^{-1}\left(\frac{y - y_\mathrm{d}}{x - x_\mathrm{d}}\right). \tag{4}$$

Fig. 2(a) shows a schematic representation of such a defect. As discussed below, this structure (i.e., of an unstrained defect field) is not sufficient to reconstruct the patterns observed in convection containers with different lateral boundary shapes. In Ref. [23], reconstructions of patterns were improved for a circular cell by introducing a spiral structure to the phase of a defect by adding a radial wavenumber of the form

$$\phi_\mathrm{d}(\mathbf{r}) = c\theta_\mathrm{d}(\mathbf{r}) + p|(\mathbf{r} - \mathbf{r_d})|. \tag{5}$$

Here p is called the pitch of the defect which is located at position $\mathbf{r_d} = (x_\mathrm{d}, y_\mathrm{d})$. Such a defect structure

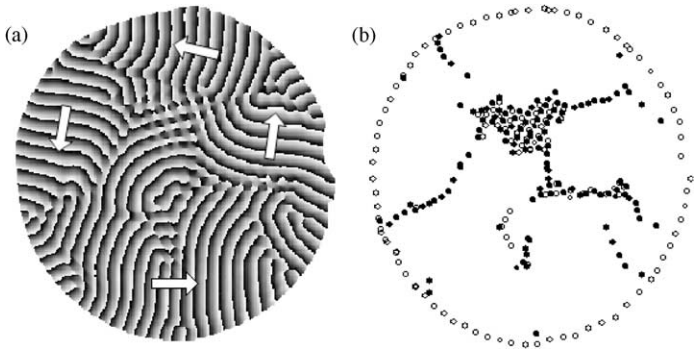

Fig. 1. (a) Map of topological defects determined from the phase field corresponding to the shadowgraph image shown in (b). The locations of the defects were determined by calculating a contour integral around each pixel in the image (see text). The full circles correspond to defects with positive topological charge and the open circles to defects with negative charge.

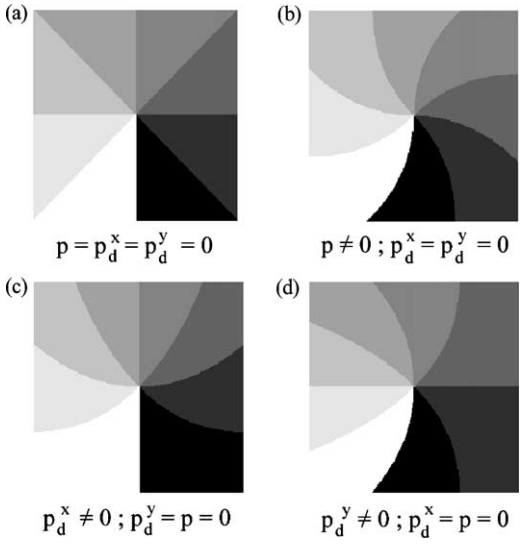

Fig. 2. Representation of the phase field of a single defect. In (a) an unstrained defect is shown. Additional structure is added to the defects: (b) a pitch giving the defect the form of a spiral; and in (c) and (d) a wavevector in the x and y directions, respectively. In reconstructions, the wavevector illustrated in (c) and (d) will point in the direction of the nearest-neighbor defect. A large value of p_d^x or p_d^y results in the familiar image of a dislocation in a wave field. Defects as illustrated in (b) occur in circular cells, while defects of the type in (c) and (d) occur in patterns in cells with broken (x, y) symmetry (e.g., rectangular cells and some patterns in stadium-shaped cells).

is shown in Fig. 2(b). This structure breaks the chiral symmetry since the charge of the defect does not influence the sense of the spiral. The breaking of chiral symmetry reflects the globally rotating nature of the patterns observed in a circular container.

However, in cells with different boundary shapes, the global structure and dynamics is qualitatively changed [24]. We found it necessary to include a local structure to single phase defects to take into account the different global symmetries of the patterns (e.g., that change qualitatively when the lateral boundary shape is changed). This is achieved by adding a local wavevector to the phase field in Eq. (5), which can be written in the form

$$\phi_d = c\theta_d + p|(\mathbf{r} - \mathbf{r_d})| + \mathbf{p_d} \cdot (\mathbf{r} - \mathbf{r_d}). \tag{6}$$

In this model, there are three adjustable parameters in the determination of the phase field of the defect, the scalar p and the two components of the vector $\mathbf{p_d}$. Examples of this parameterization are shown in Figs. 2 (c) and (d), where a defect is shown with an additional local wavevector in the x- and y-direction, respectively.

In principle, to keep track of the environment of each defect, these parameters would have to be defined locally which would lead to a plethora of adjustable parameters. However, we have found empirically that this can be avoided by defining the local wavevector and the pitch in terms of the distance of the defect from its nearest-neighbor. In the cases studied, this turns out to be predominantly a defect of the same charge, due to the fact that most defects are in domain boundaries, which are built up of like-sign defects. In these lines of defects, distances to the nearest and next nearest-neighbor can be similar. In this case, the signs of the wavevectors are likely to alternate, which over long distances, reduces the importance of this addition to the phase. However, inspection of the defect maps indicates that the lines of defects frequently exhibit significant variations in defect spacing, which helps to motivate the choice of nearest-neighbor spacing as a relevant parameter. Thus, the phases of the defects in the reconstruction are taken to be

$$\phi_d = c\theta_d + \epsilon_r|\delta||(\mathbf{r} - \mathbf{r_d})| + \epsilon_c((x - x_d)\delta_x + (y - y_d)\delta_y), \tag{7}$$

where $\delta = (\delta_x, \delta_y)$ is the distance vector to the nearest defect of the same charge. The total phase field of the pattern is obtained by taking the sum over all defects, including those along the boundary (e.g., see Fig. 1).

It should be emphasized that the parameterizations in Eqs. (6) and (7) are purely phenomenological. In particular, it is quite possible that the effect of the local environment on the structure of an individual defect can be parameterized in other ways. We do believe, however, that any structure of the individual defect should reflect the global symmetries of the overall pattern in order to be successful. As we discuss below, Eq. (7) does indeed do a reasonably good job of reconstructing a wide range of patterns in containers with widely different boundary shapes.

In Eq. (7), ϵ_c is a global scaling parameter for the wavevector of defects of charge c, and ϵ_r is a similar

global scaling parameter for the pitch independent of the defect's charge. As discussed in more detail below, the relative values (and hence importance) of these global scaling parameters depend on the global structure and dynamics of the convection patterns. These parameters are found to be related to the numbers of different defects in the pattern. For example, the value of the parameter setting the scale of the pitch of individual defects can be regarded as a measure of the breaking of chiral symmetry of the pattern as a whole. A different measure of the extent to which chiral symmetry is broken is the net charge $\mathcal{C}$ of the defects along the boundary. We find below that there is a close correspondence of $\mathcal{C}$ to the values of ϵ_r in all cells studied.

The reconstructions shown in the following are the best results obtained by changing the phenomenological parameters ϵ in Eq. (7). The quality of the reconstructions is assessed in the following way: the field of each defect is subtracted from the experimental pattern. After the subtraction, the field values have to be taken mod 2π such that a new phase field is obtained. If the agreement between the reconstruction and the pattern were perfect, a constant field (i.e., having a wavenumber of zero) would be obtained. The parameters ϵ_r, ϵ_+ and ϵ_- are adjusted to minimize the average of this wavenumber over the entire pattern. Typical values of this wavenumber for such best-fit parameters are of the order of $\sim 0.1\,\mathrm{h}^{-1}$ (i.e., $\sim$30 times smaller than the experimental wavenumber). From the influence of parameter changes on the value of this wavenumber (averaged over the whole of the cell), the errors in the values of $\epsilon_{r,c}$ are estimated to be $\sim 0.002\,\mathrm{h}^{-2}$. The reconstructions shown in the following also appear to be the best-fits according to visual comparisons of experimental patterns and reconstructions.

4. Results and discussion

We now describe the results obtained in reconstructing patterns in the various cell geometries from the positions of the defects and the model of the defect structure described above. In the course of the discussion, the relationship between the parameters introduced in Eq. (7) and the global structure and dynamics of the patterns will be elucidated.

4.1. Circular cell

The reconstruction of the phase field for a pattern in a circular convection cell is shown in Fig. 3 using both unstrained defects and the model described above. For the latter, the values of the adjustable parameters for the pitch and local wavevector are: $\epsilon_r = -0.037\,\mathrm{h}^{-2}$, $\epsilon_- = -0.006\,\mathrm{h}^{-2}$ and $\epsilon_+ = -0.030\,\mathrm{h}^{-2}$. Due to the global structures of the patterns in a circular cell, adding the freedom to choose a locally defined wavevector does not alter the reconstruction greatly.

From the values of the parameters, it can be seen that the global rotation of the pattern leads to a relatively high value of the pitch due to the spontaneous breaking in chiral symmetry. The scaling values for the local wavevectors for the defects of different sign of charge also indicate their respective numbers inside the cell. Typically one sign of charge dominates,

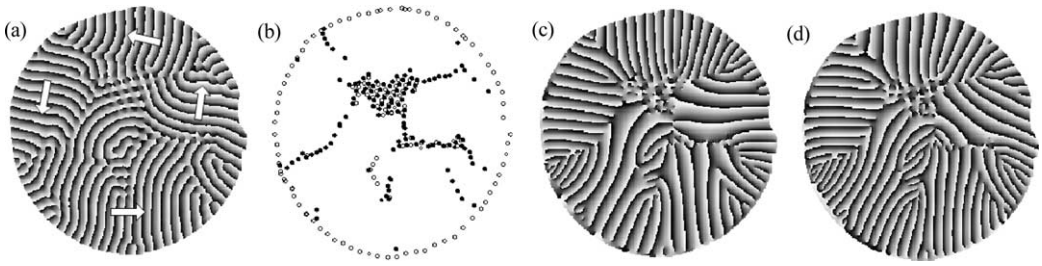

Fig. 3. Reconstructions of a pattern in the circular cell ($\Gamma = 26$). In (a) and (b) the phase field and the defect map are shown. Part (c) shows a reconstruction using unstrained defects ($\phi = c\theta$). In (d), the defects are described using Eq. (7); the values of the parameters are: $\epsilon_r = -0.037\,\mathrm{h}^{-2}$, $\epsilon_- = -0.006\,\mathrm{h}^{-2}$ and $\epsilon_+ = -0.030\,\mathrm{h}^{-2}$.

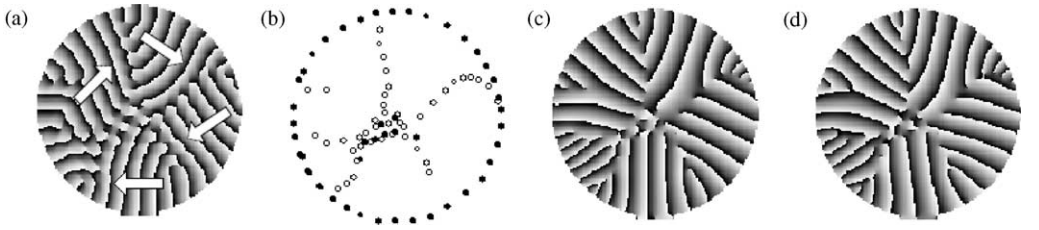

Fig. 4. (a) Pattern in a small circular cell with an aspect ratio $\Gamma = 13$. The map of defects is shown in part (b). Reconstructions are shown in (c) using unstrained defects, and in (d) using structured defects as described by Eq. (7). The values of the adjustable parameters are: $\epsilon_r = 0.018\,\mathrm{h}^{-2}$, $\epsilon_- = 0.015\,\mathrm{h}^{-2}$ and $\epsilon_+ = 0.003\,\mathrm{h}^{-2}$. Comparison of these parameters with those for the pattern analyzed in Fig. 3 indicates that they scale with the size of the cell (see text).

leading to a sizeable value of the corresponding ϵ_c. These points clarify further the previous reconstructions of traveling-wave patterns in binary fluid convection [23]. The fact that the dynamics of the defects reflect the dynamics of the pattern as a whole, made possible some prediction of defect motion based on the wavevector field. The global dynamics in the circular cell are very stable, and so the pitch and local wavevector are, to a good approximation, time independent in agreement with previous work [23].

Fig. 4 shows the reconstructions of a pattern in a smaller circular cell with an aspect ratio of $\Gamma = 13$. Investigations of patterns in this cell were used to study the size dependence of the dynamics, including the dependence of the $\epsilon_{r,c}$ parameters on cell size. The model parameterized by Eq. (7) yields $\epsilon_r = 0.018\,\mathrm{h}^{-2}$, $\epsilon_- = 0.015\,\mathrm{h}^{-2}$ and $\epsilon_+ = 0.003\,\mathrm{h}^{-2}$. Comparison with the corresponding values from the larger circular cell indicates that all parameters scale almost exactly with the size of the cell, keeping in mind that the signs ϵ_r switch, as well as that ϵ_+ and ϵ_- are interchanged. This latter point is exemplified by the patterns in Figs. 3 and 4, which rotate in opposite directions. We find $\epsilon_+/\epsilon_- = 5$ for the data in Fig. 3 and $\epsilon_-/\epsilon_+ = 5$ for Fig. 4.

4.2. Rectangular cell

The patterns in the rectangular cell are qualitatively different from those in a circular container [24]. Instead of globally rotating patterns, there is quite generally a source of traveling waves in corners of the cell. In a certain region of Rayleigh numbers, two sources can coexist which leads to patterns of the type shown in Fig. 5 (a). The corresponding defect map is shown

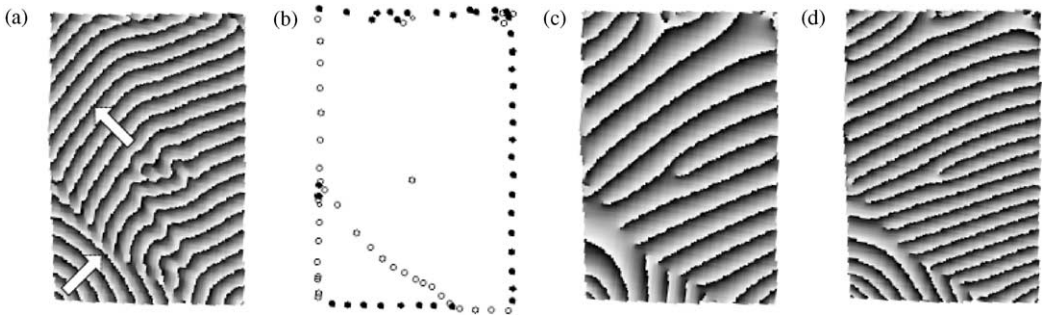

Fig. 5. Convection pattern in the rectangular cell: (a) phase field, (b) defect map; (c) and (d) are reconstructions using unstrained and structured defects, respectively. In (d), the parameters in Eq. (7) are $\epsilon_r = 0.008\,\mathrm{h}^{-2}$, $\epsilon_- = 0.054\,\mathrm{h}^{-2}$ and $\epsilon_+ = -0.043\,\mathrm{h}^{-2}$. The different values of the ϵ compared with those in the circular cells reflect the changes in the global dynamics. Instead of a global rotation of the pattern, the two sources in the corners control the dynamics of this pattern.

in part (b). As can be seen from Figs. 5 (c) and (d) the introduction of a local wavevector is necessary to obtain good agreement between the experimentally determined phase fields and the reconstructions. In particular, Fig. 5 (c) shows a reconstruction using unstrained defects, whereas part (d) presents reconstructions using a pitch and a wavevector. The parameters used in the reconstructions were: $\epsilon_r = 0.008\,\mathrm{h}^{-2}$, $\epsilon_- = 0.054\,\mathrm{h}^{-2}$ and $\epsilon_+ = -0.043\,\mathrm{h}^{-2}$. Note that the scaling parameter for the pitch, ϵ_r, is a factor of 5 smaller than in the case of the circular cell. This is consistent with the much smaller net charge, $\mathcal{C}$, of defects along the boundary corresponding to a very small breaking of chiral symmetry.

The fact that the reconstruction in Fig. 5 (c) does not reproduce the number of rolls along the boundary (which would naively be expected) is due to the highly non-local effects produced by the summation of the phase field of many defects. In accord with Eq. (4), all defects influence each spatial location in the same way. The result is that the singularities imposed by each defect are only guaranteed to be important on very short distances from the defects as can be seen from closer inspection of Fig. 5.

In the case where only one source dominates the pattern, chiral symmetry is not broken, and the value of ϵ_r used to obtain good reconstructions is consistent with a value of zero.

4.3. Stadium cell

The qualitative difference between the reconstruction parameters for rotating patterns in the circular cell and source-dominated patterns was investigated further by studying patterns in the stadium-shaped cell, in which a variety of different types of dynamics are observed. The dynamics in the stadium cell are in some sense intermediate between those of the circular and rectangular cells [24]. Depending on the Rayleigh number as well as the initial conditions of the convecting state, both globally rotating patterns and source-dominated patterns are observed. Examples of these can be seen in Figs. 6 and 7, where a globally rotating pattern and one dominated by a single source are presented. In the globally rotating pattern, the parameters used to obtain the reconstruction are similar to those used in the circular cell: $\epsilon_r = -0.03\,\mathrm{h}^{-2}$, $\epsilon_- = -0.012\,\mathrm{h}^{-2}$ and $\epsilon_+ = -0.018\,\mathrm{h}^{-2}$. Given the similarity of the defect arrangements which reflect the global dynamics, this is consistent with the discussion above. If one also considers that a correction to these values due to the size of the cell would be necessary for a proper comparison (i.e., as in the case of the two circular cells), the agreement in the value of ϵ_r is excellent.

In contrast, the pattern shown in Fig. 7 is similar to patterns observed in the rectangular cell, and the

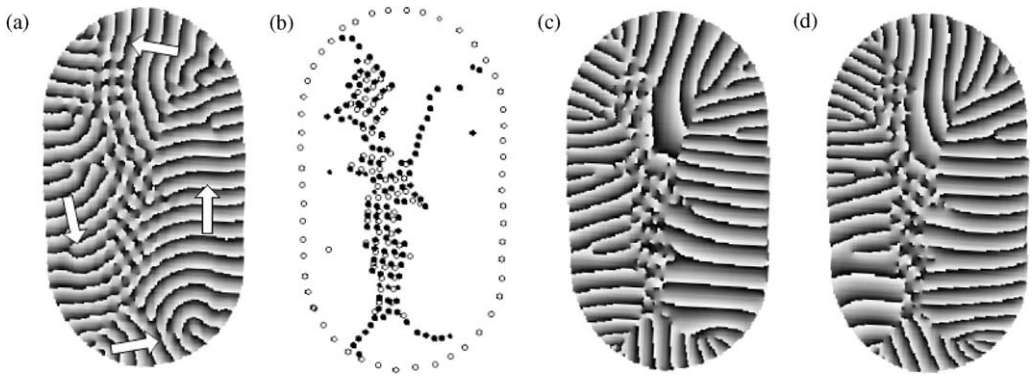

Fig. 6. Pattern observed in a stadium-shaped cell. Due to the choice of initial conditions and the strength of driving, this pattern rotates globally. (a) Phase field, (b) defect map; (c) and (d) are reconstructions using unstrained and structured defects, respectively. The parameters used in the reconstruction in (d) are: $\epsilon_r = -0.030\,\mathrm{h}^{-2}$, $\epsilon_- = -0.012\,\mathrm{h}^{-2}$ and $\epsilon_+ = -0.018\,\mathrm{h}^{-2}$. These values are similar to those for the pattern in a circular cell shown in Fig. 3.

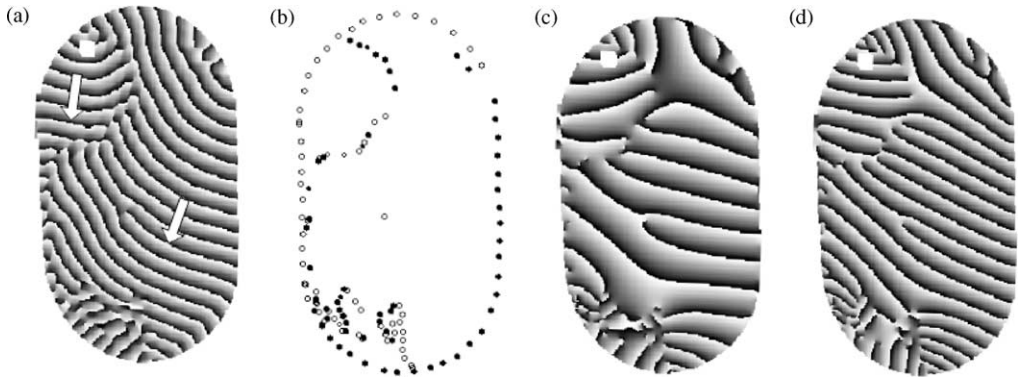

Fig. 7. A pattern in the stadium-shaped cell. In this case, the choice of initial conditions and the strength of driving are such that the pattern is dominated by sources of traveling waves on the boundary and the pattern does not rotate: (a) phase field, (b) defect map; (c) and (d) are reconstructions using unstrained and structured defects, respectively. The parameters used in the reconstruction in (d) are: $\epsilon_r = 0.001\,\mathrm{h}^{-2}$, $\epsilon_- = 0.047\,\mathrm{h}^{-2}$ and $\epsilon_+ = -0.046\,\mathrm{h}^{-2}$. These values are similar to those obtained for the pattern in the rectangular cell shown in Fig. 5.

parameters in the reconstruction reflect this fact, particularly when compared to patterns in the rectangular cell dominated by a single source (i.e., $\epsilon_r = 0.001\,\mathrm{h}^{-2}$, $\epsilon_- = 0.047\,\mathrm{h}^{-2}$ and $\epsilon_+ = -0.046\,\mathrm{h}^{-2}$). The main difference between the patterns in the different cells concerns the number of defects within the convection pattern, which leads to somewhat different values of the ϵ_c and very different values of ϵ_r. Furthermore, scaling of the ϵ parameters with the size of the cells would be appropriate here also.

The relationships between the ϵ_c and ϵ_r and between $\mathcal{C}$ and ϵ_r described above are also observed in the stadium cell. This is significant since two distinctly different kinds of dynamics are observed in the same cell. It appears that the dominant feature influencing the weights of the pitch and the local wavevector is the global dynamics of the pattern. This implies that a robust algorithm to determine the values of the ϵ requires a more detailed understanding of the interplay between the statistics of defects and global pattern dynamics.

4.4. Global aspects of the reconstructions and comparison with the patterns

As can be seen from the pattern reconstructions in the different cells, the global structure of the patterns has a strong influence on the structure of individual defects. Certain symmetries are spontaneously broken in the patterns, such as the chiral symmetry in the globally rotating patterns and (x, y) symmetry in the non-rotating patterns in the stadium and the rectangle. These symmetries are reflected in the structure of the individual defects required to reconstruct the patterns. Apart from the pitch, which was added to the structure of the defects to address the breaking of chiral symmetry, it was found that a local wavevector needs to be added to the defects, when the (x, y) symmetry is broken (e.g., in cases where the pattern consists of traveling waves moving preferentially in one direction).

We now discuss in more detail the relationships between the parameters in the reconstructions. The pitch, ϵ_r, scales linearly with the net charge of defects inside the cell. Thus

$$\epsilon_r = \eta\mathcal{C}, \tag{8}$$

where η is a constant to be determined. This relationship can be seen from the reconstructions in two circular cells of aspect ratio $\Gamma = 13$ and 26, respectively. In these cells, the values of $\epsilon_{r,c}$ used in the reconstruction scale linearly in Γ, as was discussed in Section 4.1.

Table 1 summarizes data from the different convection cells, including the numbers of defects in the cells ($\mathcal{N}_c$) and on the boundaries ($\mathcal{N}_{\mathrm{tot}}$), and the ϵ parameters from the reconstructions. The table also shows

Table 1
Comparison of numbers of defects and reconstruction parameters for different patterns and cells[a]

Pattern dynamics	$\mathcal{N}_+$	$\mathcal{N}_-$	$\mathcal{N}_{\rm tot}$	ϵ_+	$\frac{1}{2}(\mathcal{N}_+ - \Lambda)$	ϵ_-	$\frac{1}{2}(\Lambda - \mathcal{N}_-)$	ϵ_r	$\mathcal{C}/2$
Circle ($\Gamma = 26$)	54	126	72	−31	−30.5	−6	−5.5	−37	−36
Circle ($\Gamma = 13$)	43	8	36	3	−6	15	23.5	18	18
Stadium, source	36	36	58	−46	−30	47	30	1	0
Stadium, rotation	70	125	57	−18	−15	−12	−12.5	−30	−27.5
Rectangle, two sources	20	5	59	−43	−39	54	46.5	8	7.5
Rectangle, one source	6	6	49	−42	−39.5	41	39.5	−1	0

[a] The values of the ϵ parameters are given in units of $10^{-3}\,\mathrm{h}^{-2}$. The measured parameters are $\mathcal{N}_{\rm tot}$, which is the total number of defects along the cell boundary, and $\mathcal{N}_c$, the numbers of defects of charge c inside the cell; $\mathcal{C} = \mathcal{N}_+ - \mathcal{N}_-$. With a value of $\eta = (1/2) \times 10^{-3}\,\mathrm{h}^{-2}$, there is excellent agreement between $\eta\mathcal{C}$ and ϵ_r in all cases. The values of $\eta c(\mathcal{N}_c - \Lambda)$ also correlate reasonably well with the ϵ_c. Given that the data imply $\epsilon_r = \epsilon_+ + \epsilon_-$ (i.e., Eq. (9)), all patterns can be described to a high degree of accuracy by two parameters, ϵ_+ and ϵ_-. Approximate values of these parameters in different situations can be obtained from Eq. (10) using the constant η and $\Lambda = 1.6 \times \mathcal{N}_{\rm tot}$.

that ϵ_r is $\sim\mathcal{C}/2 \times 10^{-3}\,\mathrm{h}^{-2}$, fixing the value of $\eta \simeq (1/2) \times 10^{-3}\,\mathrm{h}^{-2}$. A further correlation of the values of the adjustable parameters that can be seen in Table 1 concerns the relation between the ϵ_c and ϵ_r. In all cases investigated it was found that

$$\epsilon_r = \epsilon_+ + \epsilon_-. \tag{9}$$

While Eq. (9) by itself cannot be used to strongly constrain the values ϵ_c, taking Eq. (9) together with Eq. (8), a phenomenological expression can be written in the form

$$\epsilon_c = c\eta(\mathcal{N}_c - \Lambda). \tag{10}$$

Here $\mathcal{N}_c$ is the number of defects of charge c inside the cell, Λ is a constant to be determined, and η is the same as in Eq. (8). Inspection of the values of ϵ_+ and ϵ_- obtained from experiments (see Table 1) indicates that Λ depends on the shape and size of the cell. A natural measure of the cell size is the total number of defects, $\mathcal{N}_{\rm tot}$, along the boundary of the cell (i.e., $\mathcal{N}_{\rm tot}$ is the cell's circumference divided by $2h$). An interesting possibility is that Λ is related to $\mathcal{N}_{\rm tot}$. We found that the data are consistent with $\Lambda \simeq 1.6\mathcal{N}_{\rm tot}$, but this does not include a possible dependence on the cell shape. Furthermore, the data are not yet good enough to determine an exact relationship. Table 1 indicates, however, that the values of ϵ_c can be estimated from the values of $c(\mathcal{N}_c - \Lambda)$, where Λ is given by the above estimate $\Lambda \simeq 1.6\mathcal{N}_{\rm tot}$. Alternatively, Λ can be estimated independently from the values of ϵ_+ and $\mathcal{N}_+$, as well as ϵ_- and $\mathcal{N}_-$. The values obtained for both signs of charge agree, if they are evaluated from the same pattern. They are also consistent with the dependence on the total number of defects $\mathcal{N}_{\rm tot}$ discussed above. In the small circular cell, however, the determination of Λ gives a value somewhat lower than $1.6\mathcal{N}_{\rm tot}$, which is reflected by the difference between the values of ϵ_c and $c(\mathcal{N}_c - \Lambda)/2 \times 10^{-3}\,\mathrm{h}^{-2}$.

To summarize the results in Table 1, the measured quantities are the number of defects in the patterns of each sign of charge, $\mathcal{N}_+$ and $\mathcal{N}_-$, and the total number of defects on the cell boundary, $\mathcal{N}_{\rm tot}$. We find that, given the constraint of Eq. (9), all of the patterns can be described by two parameters, ϵ_+ and ϵ_- (i.e., replacing ϵ_r, used previously to describe globally rotating patterns in circular cells). In turn, using the (again empirical) observation, Eq. (10), ϵ_+ and ϵ_- can be determined by η and a parameter, Λ, which is given approximately by $\Lambda = 1.6\mathcal{N}_{\rm tot}$.

Although the reconstructions capture the overall structure of the patterns in all of the cell geometries studied, certain elements are still missing. Most pronounced is the extreme rigidity of the wavenumber observed in the experiments. This can be seen directly in the experimental images of the patterns and also from the wavenumber distributions of the patterns, which are shown in Fig. 8. As can be seen in this figure, the reconstruction techniques described here do a relatively poor job of reproducing the narrow wavenumber distributions observed in the case of a rotating pattern. Thus some

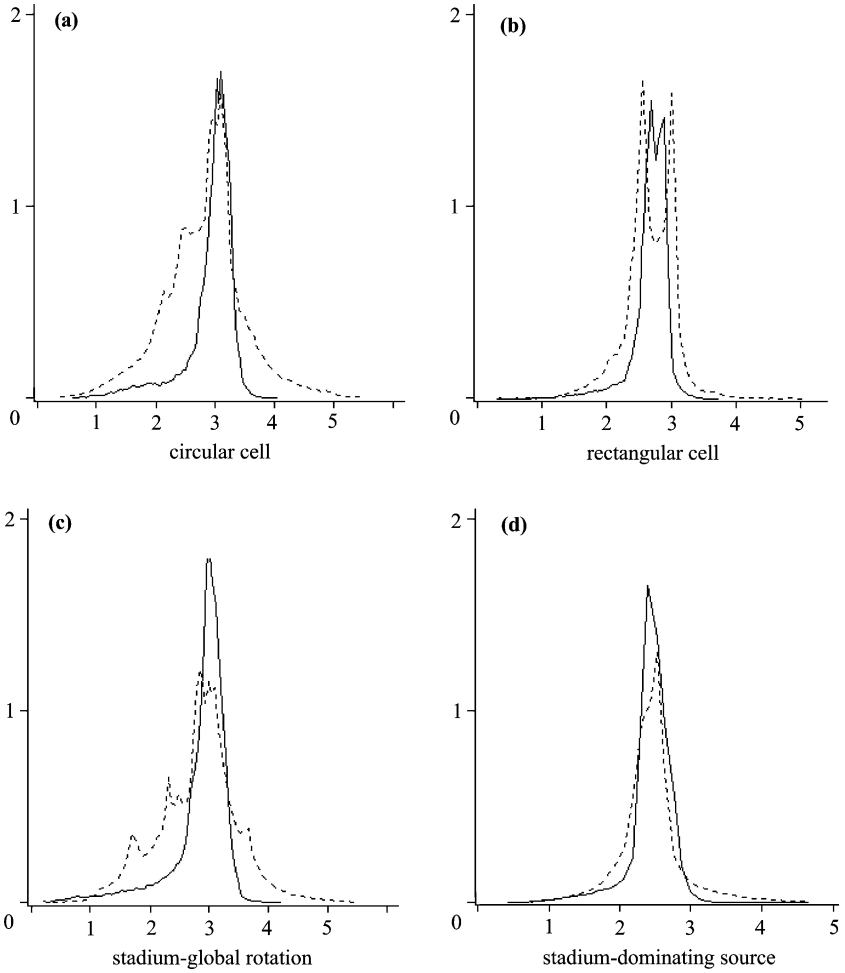

Fig. 8. The wavenumber distributions in arbitrary units for the patterns and reconstructions presented in Fig. 3 (part a), Fig. 5 (part b), Fig. 6 (part c) and Fig. 7 (part d). In cases where the pattern exhibits global rotation, the wavenumber spreads in the experimental patterns are much narrower than those in the reconstructions. In parts (b) and (d), the reconstructions fit better, but there are still discrepancies between the observations and the reconstructions (see text).

additional mechanism must be involved, which is not included in this phase-defect description. One such mechanism is phase diffusion which would tend to smooth out the phase field. It is unclear at present how this might be incorporated in a phase-defect model.

5. Conclusions

We have shown that traveling-wave patterns in binary fluid convection can be described in terms of the locations of topological defects in the phase of the complex order parameter. Such a reconstruction of the phase field from the defects is one of the necessary ingredients in a ‘particle-field’ description, which is a candidate for a much simplified description of the patterns and dynamics of non-equilibrium pattern forming systems [19,23]. For an accurate representation of the patterns in different geometries, we find that the phase field of a single defect depends on nearest-neighbor interactions in a manner associated with the global structure of the pattern.

Thus the structure of a single defect reflects the symmetry of the global pattern. In the reconstructions described here, this is modeled by the statistics of the defects (cf., Table 1). However in obtaining the reconstructions, the weights of the pitch and the local wavevector of the defects were treated as phenomenological parameters. An open question is whether some kind of theoretical model can be constructed that reflects the relationships implied by Table 1. In addition, the wavenumber distributions obtained in the reconstructions are broader than those of the experimental patterns, in cases where the patterns rotate globally. Thus some additional mechanism, not included in the present phase-defect description (such as phase diffusion), appears to be involved in determining the patterns.

The overall success of this phase-defect approach in describing complicated traveling-wave patterns in a variety of circumstances and with very different global dynamics is promising. In this description, the number of parameters needed to describe a pattern is decreased dramatically to just one or two parameters beyond the locations and signs of the defects. The problem is essentially reduced to a many-body problem of the interactions of the defects, while the structure of the phase at a single defect reflects the symmetry of the pattern as a whole. It might be possible to construct a self-consistent description of these symmetries in terms of the distribution of the phase defects in the cell which, in turn, could lead to a reconstruction of the patterns without the need for phenomenological parameters. The more ambitious goal is to attempt to use this knowledge of the patterns to predict the dynamics of the system using, for example, an approach similar to that described in Ref. [23] for the patterns in a circular cell.

Acknowledgements

We would like to acknowledge Arthur La Porta for helpful conversations. This work was supported by the US Department of Energy under Grant No. DE-FG03-ER14148.

References

[1] M.C. Cross, P.C. Hohenberg, Rev. Mod. Phys. 65 (1993) 851.
[2] P. Manneville, Dissipative Structures and Weak Turbulence, Academic Press, Boston, MA, 1990.
[3] H.M. Jaeger, S.R. Nagel, R.P. Behringer, Rev. Mod. Phys. 68 (1996) 1259 and references cited therein.
[4] S. Chandrasekar, Hydrodynamic and Hydromagnetic Stability, Clarendon Press, Oxford, 1961.
[5] St. Hollinger, M. Lücke, Phys. Rev. E 57 (1998) 4238.
[6] A.N. Zaikin, A.M. Zhabotinskii, Nature 225 (1970) 535; Q. Ouyang, H.L. Swinney, Nature 352 (1991) 610.
[7] A.M. Turing, Phil. Trans. R. Soc. B 237 (1952) 37.
[8] R. Surdeanu, R.J. Wijngaarden, B. Dam, J. Rector, R. Griessen, C. Rossel, Z.F. Ren, J.H. Wang, Phys. Rev. B 58 (1998) 12467.
[9] C.M. Aegerter, Phys. Rev. E 58 (1998) 1438.
[10] P. Coullet, L. Gil, F. Rocca, Opt. Commun. 73 (1989) 403; K. Staniunas, Phys. Rev. A 48 (1993) 1573; J. Lega, J.V. Moloney, A.C. Newell, Phys. Rev. Lett. 73 (1994) 2978.
[11] F. Pociot, B. Freisleben, P. Bak, A.E. Karlsen, Diabetes 47 (1998) 846.
[12] R.M. May, Nature 261 (1974) 459; P. Kareiva, U. Wennergren, Nature 373 (1995) 299.
[13] H. Levine, W. Reynolds, Phys. Rev. Lett. 66 (1991) 2400; E. Ben-Jacob, O. Shochet, A. Tenenbaum, I. Cohen, A. Czirok, T. Vicsek, Nature 368 (1994) 46.
[14] J.J. Bonner, The Cellular Slime Molds, Princeton University Press, Princeton, NJ, 1967.
[15] L. Glass, P. Hunter, Physica D 43 (1990) 1; J. Jalife (Ed.), Mathematical Approaches to Cardiac Arrythmias, Ann. NY Acad. Sci. 591 (1990); A.L. Hodgkin, A.F. Huxley, J. Physiol. 117 (1952) 500.
[16] P. Kolodner, J.A. Glazier, H. Williams, Phys. Rev. Lett. 65 (1990) 1579.
[17] E. Bodenschatz, W. Pesch, L. Kramer, Physica D 32 (1988) 135.
[18] I. Rehberg, S. Rasenat, V. Steinberg, Phys. Rev. Lett. 62 (1988) 756.
[19] J.D. Rodriguez, L.M. Pismen, L. Sirovich, Phys. Rev. A 44 (1991) 7980.
[20] J.C. Neu, Physica D 43 (1990) 385.
[21] R.W. Walden, P. Kolodner, A. Passner, C.M. Surko, Phys. Rev. Lett. 55 (1985) 496.
[22] P. Kolodner, C.M. Surko, Phys. Rev. Lett. 61 (1988) 842.
[23] A. LaPorta, C.M. Surko, Physica D 139 (2000) 177.
[24] C.M. Aegerter, C.M. Surko, Phys. Rev. E 63 (2001) 46301.
[25] J.K. Platten, J.C. Legros, Convection in Liquids, Springer, Berlin, 1984.
[26] L.D. Landau, E.M. Lifshitz, Fluid Mechanics, Course of Theoretical Physics, Vol. 6, Pergamon Press, Oxford, 1987.
[27] P. Kolodner, H. Williams, C. Moe, J. Chem. Phys. 88 (1988) 6512.
[28] A. LaPorta, C.M. Surko, Phys. Rev. E 53 (1996) 5916.
[29] A. LaPorta, C.M. Surko, Phys. Rev. Lett. 77 (1996) 2678; A. LaPorta, C.M. Surko, Phys. Rev. E 56 (1997) 5351.